Estimates of the thermal conductivity and the thermoelectric properties of PbTiO_{3} from first principles

Anindya Roy

Phys. Rev. B **93**, 100101 — Published 9 March 2016

DOI: 10.1103/PhysRevB.93.100101

Estimates of the thermal conductivity and the thermoelectric properties of $PbTiO_3$ from first principles

Anindya Roy*
Materials Science & Engineering, Johns Hopkins University, Baltimore, MD 21218, USA
(Dated: February 24, 2016)

The lattice thermal conductivity ($\kappa_{\rm L}$) of $PbTiO_3$ (PTO) is estimated using a combination of *ab initio* calculations and semiclassical Boltzmann transport equation. The computed $\kappa_{\rm L}$ is remarkably low, nearly comparable with the $\kappa_{\rm L}$ of good thermoelectric materials such as PbTe. In addition, a semiclassical analysis of the electronic transport quantities is presented, which suggests excellent thermoelectric properties, with a figure of merit zT well over 1 for a wide range of temperature. For thermoelectric applications, the $\kappa_{\rm L}$ could be further reduced by utilizing different morphologies and compositions.

PACS numbers: 72.20.Pa, 77.84.-s, 63.20.kg, 71.15.Mb

$PbTiO_3$ (PTO) is a well studied perovskite ferroelectric, and is used extensively in the technologically important ferroelectric/piezoelectric ceramic $PbZr_xTi_{(1-x)}O_3$ (PZT). PTO transitions from the cubic paraelectric (PE) phase to the tetragonal ferroelectric (FE) phase at temperature $T_c = 763$ K. Recent computational work predicted PTO to be a promising p-type transparent conducting compound based on its electronic structure.[1] Following doping to increase electrical conductivity, we can speculate about its thermoelectric behavior. The thermoelectric figure of merit at temperature T is given by $zT = \sigma S^2 T/(\kappa_{\rm L} + \kappa_{\rm e})$, where σ is the electrical conductivity, S is the Seebeck coefficient, and $\kappa_{\rm L}$ and $\kappa_{\rm e}$ are the lattice contribution and the electronic contribution to thermal conductivity (κ). As a first approximation, the $\kappa_{\rm e}$ of semiconductors is related to σ as $\kappa_{\rm e} = L\sigma T$. The Lorenz number L is a near-constant for many materials, which leaves little room for controlling $\kappa_{\rm e}$ independent of σ. On the other hand, researchers have been pursuing many methods to reduce $\kappa_{\rm L}$ to increase zT.[2,3]

PTO has a relatively small unit cell which may not favor low $\kappa_{\rm L}$. However, it has been observed that anharmonicity, such as that seen in thermoelectrics like PbTe, can decrease $\kappa_{\rm L}$ despite small lattice constants. PTO is used in superlattices and alloys – morphologies that could enhance phonon scattering and thus reduce $\kappa_{\rm L}$ further. Despite this promise, only limited amount of experimental results are available on the topic of room-temperature and high-temperature behavior of $\kappa_{\rm L}$ in ferroelectrics including PTO.[4–6] Computational estimate of $\kappa_{\rm L}$ could illuminate some of these points. With this in mind, a semiclassical analysis of $\kappa_{\rm L}$, as well as the electronic transport parameters of PTO are reported in this paper. The calculations are based on Boltzmann transport equations (BTE), which rely on *ab initio* results as the input. This study indicates a very low $\kappa_{\rm L}$ and high thermoelectric potential for PTO.

Here DFT-based lattice dynamics methods are applied to generate the second-order interatomic force constants (IFC2), which are then used in the BTE solver (for phonons) to determine $\kappa_{\rm L}$. The lattice dynamics methods assume harmonic forces on the atoms. If the forces have large anharmonic components, the resulting IFC2 will be less accurate, which in turn will make $\kappa_{\rm L}$ less precise. Thus, IFC2 from extreme anharmonic cases, or that from dynamically unstable structures cannot be used to determine the corresponding $\kappa_{\rm L}$. For example, the cubic PTO structure for which DFT calculations predict imaginary phonon frequencies is outside the scope of the present study. However, tetragonal PTO (t-$PbTiO_3$) shows less anharmonicity under the same calculation methods, and hence provides an alternate route to study $\kappa_{\rm L}$ from first principles.

To understand if the degree of anharmonicity in t-$PbTiO_3$ is within a reasonable limit, I checked available experiments on PTO and other materials. The example of PbTe, an incipient ferroelectric and a leading thermoelectric, is particularly relevant in this context. Strong anharmonic interaction between longitudinal acoustic (LA) and transverse optic (TO) modes has been determined as the *cause* of the exceptionally low $\kappa_{\rm L}$ of PbTe.[7,8] DFT-based methods successfully estimated $\kappa_{\rm L}$ in PbTe despite such strong anharmonic interaction.[9,10] Anharmonicity in the phonon dispersion results of PTO has been studied experimentally.[11–13] By performing least-square analysis of the phonon frequencies near T_c, Freire and Katiyar concluded that anharmonicity in t-$PbTiO_3$ is small.[14] Taken together, the observations on PbTe and PTO validate the use of the DFT-based methods to determine $\kappa_{\rm L}$ for t-$PbTiO_3$. Additionally, in this work the phonon dispersion and $\kappa_{\rm L}$ are computed for different tetragonal structures of t-$PbTiO_3$ to study how structural changes affect $\kappa_{\rm L}$. This approach is similar to the recent work on PbTe and other Pb-chalcogenides by Skelton and co-workers.[10] Different t-$PbTiO_3$ structures show modest variation in $\kappa_{\rm L}$, according to the calculations presented here; and the range of $\kappa_{\rm L}$ closely follows the experimental $\kappa_{\rm L}$. This conclusion for PTO, and similar conclusions for PbTe and the related systems[10] suggest that the DFT-based determination of $\kappa_{\rm L}$ could be a robust method, applicable to other ferroelectric/antiferroelectric materials.

The DFT calculations presented in this work were performed with Vienna Abinitio Simulation Package (VASP).[15,16]

Local density approximation (LDA)-based projector-augmented wave (PAW) pseudopotentials,[17] which included the semicore p electrons of Ti, were used for these calculations. The self-consistent calculations (SCF) and ionic relaxations with fixed lattice parameters had a plane-wave cutoff of 400 eV, whereas a higher cutoff of 520 eV was applied when optimizing cell parameters. A $8 \times 8 \times 8$ Monkhorst-Pack k-point mesh was used for the Brillouin zone integration. Forces on ions were converged to less than 0.001 eV/Å. Scalar relativistic effects were included in these calculations, but the spin-orbit effect was left out. According to these calculations, relaxed cell parameter for cubic PTO is $a = 3.881$ Å. The optimized t-$PbTiO_3$ (referred to as the S_2 structure from now on) has $a = 3.856$ Å, and $c/a = 1.046$. The cell parameters and the internal coordinates of atomic positions agree well with the previously reported values obtained from DFT-LDA calculations.[18,19] Electronic density of states (eDOS) of the optimized cubic and tetragonal structures were determined via non self-consistent calculations with a k-point grid of $30 \times 30 \times 30$. The top valence bands of PTO (both in tetragonal and cubic structures) show strong dispersive character and are formed by the hybridization between Pb $6s^2$- and O $2p^6$-like orbitals, whereas the bottom of the conduction bands are relatively flat and have large contribution from Ti $3d$-like orbitals. The eDOS calculated in this work agree with previous reports.[1,20]

Besides S_2, the phonon dispersion and κ_L were determined for three other tetragonal structures, all with relaxed ionic positions. Two of these structures have $a = 3.856$ Å with $c/a = 1.06$ (S_1) and 1.03 (S_3), whereas the third structure has $a = 3.904$ Å, and c/a =1.03 (S_4). The systematic shift in phonon frequencies was studied using these tetragonal structures, by varying the lattice parameter a while the tetragonality ratio c/a was kept fixed, and vice versa. Phonon dispersion plots were computed under stringent convergence criteria, using the Phonopy code,[21] with VASP as the DFT calculator. A set of finite displacement calculations on the $4 \times 4 \times 4$ supercells of t-$PbTiO_3$ (containing 320 atoms) produced the IFC2 used in this work.

Fig. 1 shows the phonon dispersion for the structures S_1–S_4. In this figure we zoom into the region with phonon frequencies up to 200 cm^{-1} to inspect the thermal-current-carrying, low-lying phonon branches in greater detail. The acoustic modes of S_4 have smaller frequencies ("softer") than the rest, and those belonging to S_1–S_3 nearly overlap except in the M–Γ region, where the structures with smaller c/a have lower frequencies, i.e., $\omega(S_1) > \omega(S_2) > \omega(S_3)$. Phonon frequencies of the lowest optic modes along the A–M–Γ path follow the same pattern for S_1–S_3, whereas the optic modes related to S_4 appear to have *higher* frequencies than S_1–S_3. The lowest optic mode at Γ, known as $E(TO_1)$,[22] stiffens for structures that are more tetragonal. This effect of tetragonality on the zone-center $E(TO_1)$ has been observed in previous calculations.[19] Experimental confirmation[12] of this trend

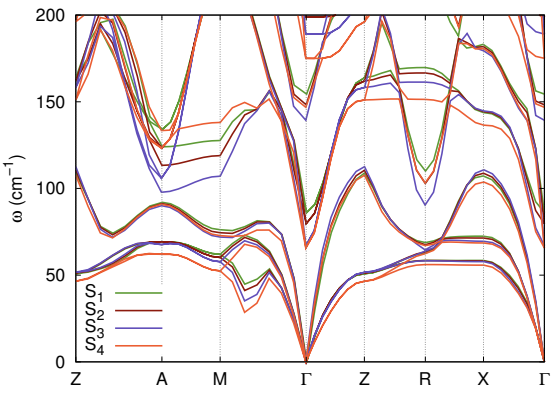

FIG. 1. (Color online) Lowest branches in the phonon dispersion for the structures S_1–S_4.

of $E(TO_1)$ is available via the temperature behavior of t-$PbTiO_3$: a rise in T that reduces the tetragonality in t-$PbTiO_3$ is found to lower the associated $E(TO_1)$ frequency. Thus the experiments and the calculations agree qualitatively.[23]

In general, a more quantitative connection between structure and T can be determined in some cases using the quasiharmonic approximation (QHA), which includes the phonon contribution to Helmholtz free energy as a function of volume (V) and T. Here we make a digression to look at the QHA analysis of t-$PbTiO_3$ before moving on to discuss κ_L calculations. QHA assumes harmonic forces on atoms at a specific volume, but allows for phonon frequencies to change with structure. Theoretical background and the implementation details of QHA are available in Refs. 10 and 24. Tetragonal symmetry in t-$PbTiO_3$ implies that the coefficient of thermal expansion (CTE), a second-rank tensor, has only two independent components, given by $\alpha_{xx} (= \alpha_{yy})$ and α_{zz} (following the Voigt notation). The components α_{xx} and α_{zz} are related to the principal components of strain as $\epsilon_{xx} = \alpha_{xx}\Delta T$, and $\epsilon_{zz} = \alpha_{zz}\Delta T$.[25] The volume CTE is $\alpha_V = 2\alpha_{xx} + \alpha_{zz}$. PTO shows negative thermal expansion (NTE) between ~300 K–T_c.[26–28] As T rises towards T_c, the c/a of t-$PbTiO_3$ decreases (as alluded to briefly in the last paragraph) while a increases slightly, with an overall reduction in volume. Past attempts at applying QHA to determine the thermal expansion in PTO have run into difficulties. In one case, α_V came out to be positive,[29] whereas another study reported a vastly overestimated magnitude of α_V.[30] In general, the lattice parameters of t-$PbTiO_3$ change in complex ways as functions of pressure,[31–34] which may be partly responsible for the difficulty in matching the QHA results for t-$PbTiO_3$ with the experimental CTE.

In this work, the directly comparable components of CTE would be those determined under epitaxial constraints, because the phonon dispersion of different tetragonal structures (S_1–S_4) were compared by changing either the in-plane (x and y) or the out-of-plane (z)

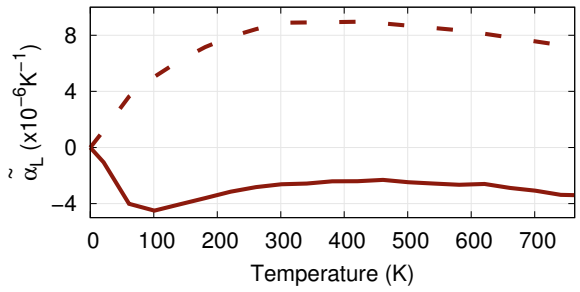

FIG. 2. CTE components for t-$PbTiO_3$ as a function of temperature. The solid (lower) and the dashed (upper) curves represent $\tilde{\alpha}_{zz}$ and $\tilde{\alpha}_{xx}$, respectively.

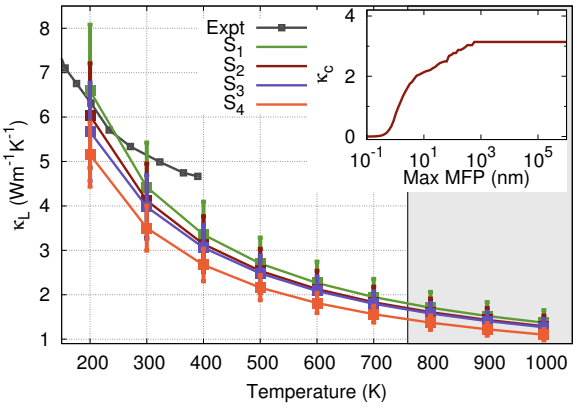

FIG. 3. (Color online) κ_L as a function of T for the S_1–S_4 structures of t-$PbTiO_3$, along with the experimental data from Ref. 6. The upper bound and the lower bound of the bars represent the κ_L values along the in-plane and the out-in-plane axes, whereas the solid line represents one-third the trace of κ_L. The region corresponding to $T > T_c$ is shaded in grey. Cumulative κ_L is expressed as a function of maximum mean free path for the S_2 structure at 400 K (inset).

lattice direction(s), while holding the other fixed. The resulting CTE components can be termed *clamped* coefficients, $\tilde{\alpha}_{xx}$ and $\tilde{\alpha}_{zz}$, which are not the same as α_{xx} and α_{zz}. The Phonopy-QHA code[21] was used to compute $\tilde{\alpha}_{xx}$ and $\tilde{\alpha}_{zz}$. To determine $\tilde{\alpha}_{xx}$, a total of 12 structures were studied which spanned a variation in a by $\pm 0.5\%$ around the optimized a of t-$PbTiO_3$ (while the optimized c was held fixed). Similarly, $\tilde{\alpha}_{zz}$ was obtained using 11 structures by varying c in a range of -0.3% to 0.7% around the optimized c, while a remained fixed. In Fig. 2 we see that in the 300 K–600 K, $\tilde{\alpha}_{xx}$ is $\sim 9\times10^{-6}$ °C^{-1} and $\tilde{\alpha}_{zz}$ is $\sim -3\times10^{-6}$ °C^{-1}. The phonon dispersion results for S_1–S_4 structures along with the computed values of $\tilde{\alpha}_{xx}$ and $\tilde{\alpha}_{zz}$ firmly establish that the structures with smaller c/a ratio correspond to higher T in these calculations.

Having explored how the S_1–S_4 structures relate to T, we now proceed to the results of the κ_L calculations. The ShengBTE code[35,36] used in this work iteratively solves BTE for phonons to determine κ_L. The IFC2 required in this code were obtained using the Phonopy code as described earlier, generated with $4\times4\times4$ supercells via finite difference approach. The anharmonic IFC3 were obtained using the code thirdorder.py[37] (supplied with ShengBTE), following the same finite difference methods on $3\times3\times3$ t-$PbTiO_3$ supercells. Interaction up to the third nearest neighbors was included in these calculations, and VASP was used as the DFT engine. The linearized BTE was solved on a Γ-centered, $16\times16\times16$ q-point grid, which sufficiently converged κ_L. The supercells considered above to generate the set of IFC2 and IFC3 adequately converged κ_L. To test the convergence of κ_L on supercell size, additional sets of IFC2 and IFC3 were generated for the S_2 structure, on supercells of dimensions $3\times3\times3$ and $2\times2\times2$, respectively. Including the original choice ($4\times4\times4$ supercells for IFC2, and $3\times3\times3$ supercells for IFC3), four combinations of IFC2 and IFC3 were tested. For S_2, κ_L calculated with these four combinations lie within 0.2 $Wm^{-1}K^{-1}$, accurate enough for the purpose of this work.

Fig. 3 shows the κ_L values for the structures S_1–S_4, with the shaded region corresponding to values of κ_L for $T > T_c$ determined based on the tetragonal structure. First, we note that κ_L in PTO is low, especially at high temperature, and the structures with smaller c/a show a lower κ_L. This effect is most pronounced for S_4, whereas the curves corresponding to S_1–S_3 show significant overlap. The structural dependence of κ_L in t-$PbTiO_3$ indicates that anharmonicity strongly affects κ_L. The experimental thermal conductivity results on perovskite ferroelectric samples[4,6] suggest that structural phase transitions do not significantly change the overall T dependence of κ_L, except for a discontinuity close to T_c. This observation was used to calculate κ_L beyond T_c using IFC2 and IFC3 corresponding to tetragonal structures. The top and the bottom end of the bars in Fig. 3 correspond to the κ_L values along the in-plane and the out-of-plane axes respectively, while the solid line represents the one-third the trace of the κ_L tensor. The inset of Fig. 3 shows the cumulative κ_L as a function of the maximum phonon mean free path for the optimized t-$PbTiO_3$ structure (S_2) at 400 K. According to these calculations, a nanoparticle of 10 nm diameter will have κ_L of about 2 $Wm^{-1}K^{-1}$ – two thirds of its saturation value. Thus nanostructuring PTO may provide another route to reduce κ_L on top of its already low κ_L.

A comparison with the available experimental data for PTO shows overall agreement,[6] although the computed κ_L appears underestimated in the 250 K–400 K. Experimental results include κ_e, partly explaining the difference. Another contribution to this mismatch may be due to ignoring the spin-orbit effect in the calculations, reported to be important in certain cases.[9] A third source of the difference could be a result of using harmonic approximation to calculate the phonon dispersion, which predicted (spuriously) smaller frequencies for the low-lying TO modes. This may have assigned a larger fraction of the thermal current to the TO modes in the present calculations. The optic modes in general have slower group

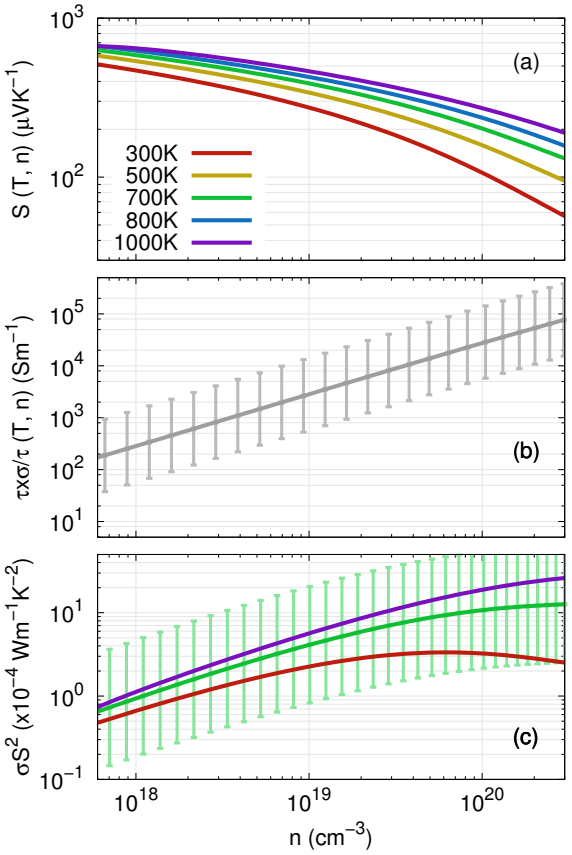

FIG. 4. (Color online) Calculated thermoelectric parameter values: (a) $S(T, n)$ for five temperatures, (b) $\sigma/\tau \times \tau$ for three representative values of τ: The solid line, and the upper and the lower limits of the vertical bars represent 5 fs, 25 fs, and 1 fs, respectively. (c) Power factor σS^2 for systems at 300 K, 700 K, and 1000 K. The bars represent the same range of τ as in panel (b) for the 700 K curve [Same legends as (a)].

velocity. Thus, a bigger fraction of the heat current carried by optic modes would lower $\kappa_{\rm L}$ overall.[38] A conclusive insight would require observations from more experiments, and calculations that consider anharmonicity explicitly.

The low $\kappa_{\rm L}$ estimated for t-$PbTiO_3$ would make it a promising thermoelectric candidate if its electronic transport properties are good enough. To this end, semiclassical Boltzmann theory-based BoltzTraP[39] code was used to estimate S, σ, and $\kappa_{\rm e}$, within the constant scattering time approximation (CSTA). In CSTA, σ and $\kappa_{\rm e}$ are determined within a factor of the scattering time τ, considered a parameter, whereas S has no such dependence on τ. Experimental results on σ, mobility and carrier concentration can be used to approximate τ. However, such experimental results are lacking for conductive samples of PTO. As a substitute, a broad range of τ, from 1 fs (=10^{-15} s) to 25 fs, was used in these calculations.

Fig. 4(a)-(c) show the calculated values of S, σ/τ, and the power factor σS^2, all presented as functions of the carrier density n. In these calculations $\kappa_{\rm e}$ was found to be small ($\leq$0.5 Wm^{-1}K^{-1} with τ = 5 fs) compared to $\kappa_{\rm L}$, and hence ignored in further discussions. The DFT-derived eDOS were obtained from the cubic or the tetragonal structure, for $T \geq T_c$ and $T < T_c$, respectively; and were interpolated by a factor of 100 for the transport calculations. For the t-$PbTiO_3$ structure, one-third the trace of the S and the σ tensors are presented. As is widely observed for semiconductor thermoelectrics, S increases with T (for the same n), and drops with increasing n (calculated at the same T). The σ/τ curve has no T dependence, and in panel (b) we see a representative curve, with the bars spanning a region bound by τ = 25 fs as the upper limit, to τ = 1 fs as the lower limit. The solid line is drawn with τ = 5 fs. Fig. 4(c) shows the estimated values of the power factor, which carries over the uncertainty in τ (the range of τ shown only for the T = 700 K case, the rest drawn for τ = 5 fs only). This plot indicates that σS^2 is often greater than 0.002 Wm^{-1}K^{-2} for a wide range of values of τ and n. For reference, a power factor of 0.002 Wm^{-1}K^{-2} at 1000 K, accompanied by a κ value of 1.15 Wm^{-1}K^{-1}, indicates a zT of 1.7 – highly promising as an initial estimate.

To summarize this work, the calculations presented here suggest that the $\kappa_{\rm L}$ for PTO is very low, possibly influenced by anharmonicity. Although these results largely agree with the experimental trends, calculations that consider anharmonic effects explicitly are expected to produce better agreement with the experiments. The low $\kappa_{\rm L}$ and the accompanying favorable electronic transport values indicate great promise of PTO as a thermoelectric material. However, this would require the electrical conductivity of PTO to be raised significantly through doping, and may call for considerable experimental effort. PTO and related perovskite functional materials have been synthesized and characterized in a variety of morphologies and compositions. Thus, processes such as alloying or increasing the complexity of the unit cell, among other measures, could be utilized to further reduce $\kappa_{\rm L}$. Synthesizing PTO in disordered structure may provide another route to reduce $\kappa_{\rm L}$ while maintaining high σ. The top of the valence band of PTO is formed by the hybridization between the Pb 6s and the O 2p orbitals. The expansive, anisotropic Pb 6s orbitals may allow band-like hole conduction even in the absence of crystalline order, an idea originally suggested in the context of n-type amorphous transparent conducting oxides.[40] This idea has recently been proposed as a means to reduce $\kappa_{\rm L}$ in ZnO-based n-type thermoelectrics.[41] The present work demonstrates that $\kappa_{\rm L}$ can be computed for the low-symmetry, dynamically stable phases of ferroelectric/antiferroelectric materials. Comparison with experiments indicates that, via extrapolation, the $\kappa_{\rm L}$ of the low-symmetry structures could be used to approximate the $\kappa_{\rm L}$ of the high-symmetry structures reasonably well.

Downloadable data files related to this work are available at `https://goo.gl/30eGtV`

ACKNOWLEDGMENTS

The author is grateful to Michael L. Falk for the discussions and the support, to Jesús Carrete for the discussions regarding the implementation of ShengBTE, and to Olivia Alley for the suggestions on the manuscript. The work was supported by NSF grant DUE-1237992. This project used the computational resources of Extreme Science and Engineering Discovery Environment (XSEDE), which is supported by NSF grant number ACI-1053575; and The Maryland Advanced Research Computing Center (MARCC) supported by the State of Maryland.

* aroy21@jhu.edu

[1] G. Hautier, A. Miglio, G. Ceder, G.-M. Rignanese, and X. Gonze, Nat. Commun. **4**, 2292 (2013).
[2] G. J. Snyder and E. S. Toberer, Nat. Mater. **7**, 105 (2008).
[3] M. W. Gaultois and T. D. Sparks, Appl. Phys. Lett. **104**, 113906 (2014).
[4] A. J. H. Mante and J. Volger, Phys. Lett. A **24**, 139 (1967).
[5] B. A. Strukov and A. A. Belov, Phase Transitions **51**, 175 (1994).
[6] M. Tachibana, T. Kolodiazhnyi, and E. Takayama-Muromachi, Appl. Phys. Lett. **93**, 092902 (2008).
[7] J. An, A. Subedi, and D. Singh, Solid State Commun. **148**, 417 (2008).
[8] O. Delaire, J. Ma, K. Marty, A. F. May, M. A. McGuire, M.-H. Du, D. J. Singh, A. Podlesnyak, G. Ehlers, M. D. Lumsden, and B. C. Sales, Nat. Mater. **10**, 614 (2011).
[9] Z. Tian, J. Garg, K. Esfarjani, T. Shiga, J. Shiomi, and G. Chen, Phys. Rev. B **85**, 184303 (2012).
[10] J. M. Skelton, S. C. Parker, A. Togo, I. Tanaka, and A. Walsh, Phys. Rev. B **89**, 205203 (2014).
[11] G. Shirane, J. D. Axe, J. Harada, and J. P. Remeika, Phys. Rev. B **2**, 155 (1970).
[12] G. Burns and B. A. Scott, Phys. Rev. B **7**, 3088 (1973).
[13] C. M. Foster, Z. Li, M. Grimsditch, S.-K. Chan, and D. J. Lam, Phys. Rev. B **48**, 10160 (1993).
[14] J. D. Freire and R. S. Katiyar, Phys. Rev. B **37**, 2074 (1988).
[15] G. Kresse and J. Furthmüller, Phys. Rev. B **54**, 11169 (1996).
[16] G. Kresse and D. Joubert, Phys. Rev. B **59**, 1758 (1999).
[17] P. E. Blöchl, Phys. Rev. B **50**, 17953 (1994).
[18] A. García and D. Vanderbilt, Phys. Rev. B **54**, 3817 (1996).
[19] P. Marton and J. Hlinka, Phase Transitions **86**, 200 (2013).
[20] S. Piskunov, E. Heifets, R. Eglitis, and G. Borstel, Comput. Mater. Sci. **29**, 165 (2004).
[21] A. Togo and I. Tanaka, Scr. Mater. **108**, 1 (2015).
[22] Conventional terminology, based on the decomposition of vibrational representation at Γ. See Ref. 18 for details.
[23] In real life, strong anharmonic forces associated with the ferroelectric transition renormalize the phonon frequencies to real values, as PTO transitions to cubic structure.
[24] S. Baroni, S. De Gironcoli, A. Dal Corso, and P. Giannozzi, Rev. Mod. Phys. **73**, 515 (2001).
[25] J. F. Nye, *Physical properties of crystals: their representation by tensors and matrices* (Oxford university press, 1985).
[26] G. Shirane, S. Hoshino, and K. Suzuki, Phys. Rev. **80**, 1105 (1950).
[27] G. Shirane and S. Hoshino, J. Phys. Soc. Jpn. **6**, 265 (1951).
[28] J. Chen, X. Xing, R. Yu, and G. Liu, J. Am. Ceram. Soc. **88**, 1356 (2005).
[29] L. Wang, P. Yuan, F. Wang, E. Liang, Q. Sun, Z. Guo, and Y. Jia, Mater. Res. Bull. **49**, 509 (2014).
[30] F. Wang, Y. Xie, J. Chen, H. Fu, and X. Xing, Appl. Phys. Lett. **103**, 221901 (2013).
[31] S. Tinte, K. M. Rabe, and D. Vanderbilt, Phys. Rev. B **68**, 144105 (2003).
[32] J. Frantti, Y. Fujioka, and R. M. Nieminen, J. Phys. Chem. B **111**, 4287 (2007).
[33] P. Ganesh and R. E. Cohen, J. Phys. Condens. Matter **21**, 064225 (2009).
[34] J. Zhu, J. Zhang, H. Xu, S. C. Vogel, C. Jin, J. Frantti, and Y. Zhao, Sci. Rep. **4** (2014).
[35] W. Li, N. Mingo, L. Lindsay, D. A. Broido, D. A. Stewart, and N. A. Katcho, Phys. Rev. B **85**, 195436 (2012).
[36] W. Li, J. Carrete, N. A. Katcho, and N. Mingo, Comp. Phys. Commun. **185**, 1747 (2014).
[37] W. Li, L. Lindsay, D. A. Broido, D. A. Stewart, and N. Mingo, Phys. Rev. B **86**, 174307 (2012).
[38] E. S. Toberer, L. L. Baranowski, and C. Dames, Annu. Rev. Mater. Res. **42**, 179 (2012).
[39] G. K. H. Madsen and D. J. Singh, Comput. Phys. Commun. **175**, 67 (2006).
[40] H. Hosono, J. Non-Cryst. Solids **352**, 851 (2006).
[41] A. Roy, Y.-T. Cheng, and M. L. Falk, J. Phys. Chem. C **120**, 2529 (2016).